Atomic structure of the vimentin central α-helical domain and its implications for intermediate filament assembly

Anastasia A. Chernyatina[a], Stefan Nicolet[a], Ueli Aebi[b], Harald Herrmann[c], and Sergei V. Strelkov[a,1]

[a]Laboratory for Biocrystallography, Department of Pharmaceutical and Pharmacological Sciences, Katholieke Universiteit Leuven, Herestraat 49, B-3000 Leuven, Belgium; [b]M. E. Müller Institute for Structural Biology, Biozentrum, University of Basel, Klingelbergstrasse 50/70, CH-4056 Basel, Switzerland; and [c]Group Functional Architecture of the Cell, German Cancer Research Center, Im Neuenheimer Feld 280, D-69120 Heidelberg, Germany

Edited by Eckhard Mandelkow, Max-Planck-Unit for Structural Molecular Biology, Hamburg, Germany, and accepted by the Editorial Board July 10, 2012 (received for review April 24, 2012)

Together with actin filaments and microtubules, intermediate filaments (IFs) are the basic cytoskeletal components of metazoan cells. Over 80 human diseases have been linked to mutations in various IF proteins to date. However, the filament structure is far from being resolved at the atomic level, which hampers rational understanding of IF pathologies. The elementary building block of all IF proteins is a dimer consisting of an α-helical coiled-coil (CC) "rod" domain flanked by the flexible head and tail domains. Here we present three crystal structures of overlapping human vimentin fragments that comprise the first half of its rod domain. Given the previously solved fragments, a nearly complete atomic structure of the vimentin rod has become available. It consists of three α-helical segments (coils 1A, 1B, and 2) interconnected by linkers (L1 and L12). Most of the CC structure has a left-handed twist with heptad repeats, but both coil 1B and coil 2 also exhibit untwisted, parallel stretches with hendecad repeats. In the crystal structure, linker L1 was found to be α-helical without being involved in the CC formation. The available data allow us to construct an atomic model of the antiparallel tetramer representing the second level of vimentin assembly. Although the presence of the nonhelical head domains is essential for proper tetramer stabilization, the precise alignment of the dimers forming the tetramer appears to depend on the complementarity of their surface charge distribution patterns, while the structural plasticity of linker L1 and coil 1A plays a role in the subsequent IF assembly process.

X-ray crystallography | cytoskeleton | coiled coil

Together with actin filaments and microtubules, intermediate filaments (IFs) constitute the three principal filament systems in metazoan cells (1, 2). It has been suggested early on that IFs form the cytoskeleton proper, serving mainly mechanical functions (3). In contrast to the globular actins and tubulins, IF proteins are fibrous molecules. In all higher metazoa they are encoded by large multigene families, accounting for approximately 70 members in man (4). Despite the fact that different IF proteins exhibit rather distinct primary structure and biochemical properties, they all share a common structural plan: A central, mostly α-helical "rod" domain of uniform size is flanked by highly variable non-α-helical "head" and "tail" domains (5). The rod domain is approximately 310 residues long in all cytoplasmic IF proteins and close to 350 residues in the nuclear ones. IF proteins have a very strong tendency to dimerize via the formation of an α-helical coiled coil (CC) by their rod domains (6). In particular, vimentin, a 53.7 kDa protein expressed mainly in cells of mesenchymal origin, reveals dimers even in 6 M urea (7). At 5 M urea, two dimers associate into a tetramer that stays as such upon further dialysis into low-salt buffer—e.g., 5 mM Tris-HCl (pH 8.4) (7, 8). These 60-nm-long tetramers result from the association of dimers in a half-staggered, antiparallel fashion so that the first halves of the rod domain are roughly aligned, the so-called "A_{11}-mode" (7, 9–12). Once the ionic strength is raised, rapid lateral association of these A_{11}-type tetramers results in the formation of so-called unit-length filaments (ULFs). Subsequently, the ULFs gradually anneal in the longitudinal direction, ultimately yielding long compacted filaments 10–12 nm in diameter.

Soon after the first IF proteins had been sequenced, the sequence-based predictions suggested that their central rod domain should contain *three* contiguous α-helical regions (13). These regions corresponded to coil 1A, coil 1B, and the complete coil 2 segment in the currently used naming scheme (14). Later on, the IF protein sequences were analyzed using algorithms that specifically search for the heptad periodicity in the distribution of apolar amino acids, which is the signature of a regular left-handed CC (6). This analysis suggested the existence of *four* regions with heptad periodicity, which led to the assumption that the rod domain contains *four* CC segments (coils 1A, 1B, 2A, and 2B) interconnected by linkers L1, L12, and L2 (15).

We aim at a better understanding of how IF proteins organize into filaments and interact with other proteins. Recently, an increasing number of reports suggested links between point mutations in various IF proteins and over 80 currently incurable human diseases, including muscle, heart, skin, and neurological disorders (16). To get a mechanistic insight into both normal and pathogenic IF behaviour, a detailed three-dimensional structure is indispensable. We are focusing on X-ray crystallographic studies of human vimentin as a "model" IF protein, using a "divide-and-conquer" approach based on the crystallization of overlapping short fragments (17). These efforts resulted in the atomic structure determination of the vimentin coil 1A [Protein Data Bank (PDB) entry *1GK7*] (18) and of several overlapping fragments covering the complete coil 2 [PDB entries *1GK6* (18), *3KLT* (19), and *3TRT* (20)]. An important conclusion of these studies was that coil 2 forms a contiguous CC structure—i.e., the linker L2 does not exist. Thus far no fragments containing significant parts of the flexible head and tail domains of any IF protein could be crystallized, with the exception of an Ig fold present within the tail domain of nuclear lamins (21).

Here, we present three previously undescribed crystal structures of human vimentin fragments that span the first half of the rod domain, including coil 1A, linker L1, and coil 1B. With these crystallographic data, the atomic structure of vimentin rod becomes essentially complete. This allows us to construct an

Author contributions: A.A.C., U.A., H.H., and S.V.S. designed research; A.A.C. and S.N. performed research; A.A.C. and S.V.S. analyzed data; and A.A.C., H.H., and S.V.S. wrote the paper.

The authors declare no conflict of interest.

This article is a PNAS Direct Submission. E.M. is a guest editor invited by the Editorial Board.

[1]To whom correspondence should be addressed. E-mail: sergei.strelkov@pharm.kuleuven.be.

This article contains supporting information online at www.pnas.org/lookup/suppl/doi:10.1073/pnas.1206836109/-/DCSupplemental.

atomic model for the vimentin tetramer and also obtain important insights into the mechanism of subsequent IF assembly.

Results

Sequence Analysis of the IF Rod Domain. As a starting point for crystallographic studies, we have revisited the prediction of the CC structure within the IF rod based on its amino acid sequence. We argue that the CC regions should comply with two criteria. Firstly, they should have a high probability of α-helix formation, as can be evaluated using standard secondary structure prediction algorithms such as Jpred3 (http://www.compbio.dundee.ac.uk/www-jpred) (22). Secondly, they should exhibit regularly spaced apolar residues forming the CC core. To this end, we have used the NetSurfP algorithm (http://www.cbs.dtu.dk/services/NetSurfP) (23) that estimates the probability for a particular residue to be buried within the hydrophobic core. While well-established CC prediction algorithms such as COILS (24) only consider the heptad periodicity typical for left-handed CCs, one should also look for other possibilities, including the 11-residue (hendecad) and 15-residue (quindecad) periodicities that drive the formation of a parallel α-helical bundle and a right-handed CC, respectively (25, 26).

We found this generalized approach to be highly accurate towards localizing the CC regions of the IF dimer. In particular, Jpred3 algorithm suggests that the first α-helical segment (coil 1A) in human vimentin should include residues 97 to 139 (Fig. 1*A*). Moreover, within the whole 1A region the buried residues indicated by the NetSurfP algorithm are in a perfect agreement with a heptad pattern (Fig. 1*A*). This very pattern is found in the crystal structure of coil-1A (*Y117L* mutant) dimer [PDB entry *3G1E* (27)]. In vimentin, the interruption of α-helical structure at linker L1 is predicted for eight residues, Gly140 to Gly147 (Fig. 1*A*). From analyzing the heptad patterns within coil 1A and coil 1B one can readily calculate that the linker L1 causes a phase shift in heptad periodicity that corresponds to an insert of five residues (or a deletion of two residues). This is distinct from either one of the two phase perturbations commonly seen within continuous CC structures, the stutter (equivalent to an insert of four residues, converting a heptad into a hendecad) or the stammer (insert of three residues) (25, 28), and also distinct from either of the inserts repeated twice. A continuous CC running from coil 1A into coil 1B is therefore highly unlikely. The length of linker L1 and, correspondingly, the phase shift at the linker are conserved throughout all type III IF proteins (Fig. 1*A*). However, in other IF types both the length and sequence of L1 vary substantially (29).

Crystal Structure of the *1AB* Fragment Corresponding to Coil 1A, Linker L1, and the First Half of Coil 1B. To obtain experimental evidence towards the L1 structure, we have crystallized the vimentin fragment *1AB*, which contains residues 99–189 and therefore spans coil 1A, linker L1, and the first half of coil 1B (Fig. 1*B*). The calculated Matthews volume of the crystals assuming two 11.1 kDa chains per asymmetric unit is 2.55 A^3/Da corresponding to 52% solvent, which implies a rather loose packing. The structure was phased experimentally by single-wavelength anomalous scattering (SAS) collected from the crystals of SeMet-containing protein (Table S1). The final structure refined against native diffraction data at 2.6 Å resolution reveals a parallel CC dimer (Fig. 2*A*). Surprisingly, a clear electron density is only observed starting from residues 144 and 149 in chains A and B, respectively. Moreover, SDS-PAGE analysis of the crystals confirmed that the fragment was intact (mass 11.1 kDa). In addition, first few traceable residues in each chain are mobile, as evident from increased B-factors. Both the coil 1A and most of the linker L1 are therefore completely disordered in this crystal structure. Tyr150 is the first residue forming the hydrophobic core of coil 1B, which has a fairly regular left-handed CC structure (Fig. 3*B*). The hydrophobic core is formed by the residues in *a* and *d* positions of the heptads in a perfect agreement with the sequence-based prediction (Fig. 1*A*). Notably, the still visible part of the linker L1 in chain A (residues 144 to 149) is also α-helical. The crystal packing arrangement is such that the 1B parts alone are sufficient to form an interconnected lattice, albeit having large voids that should be accommodating the poorly ordered 1A parts.

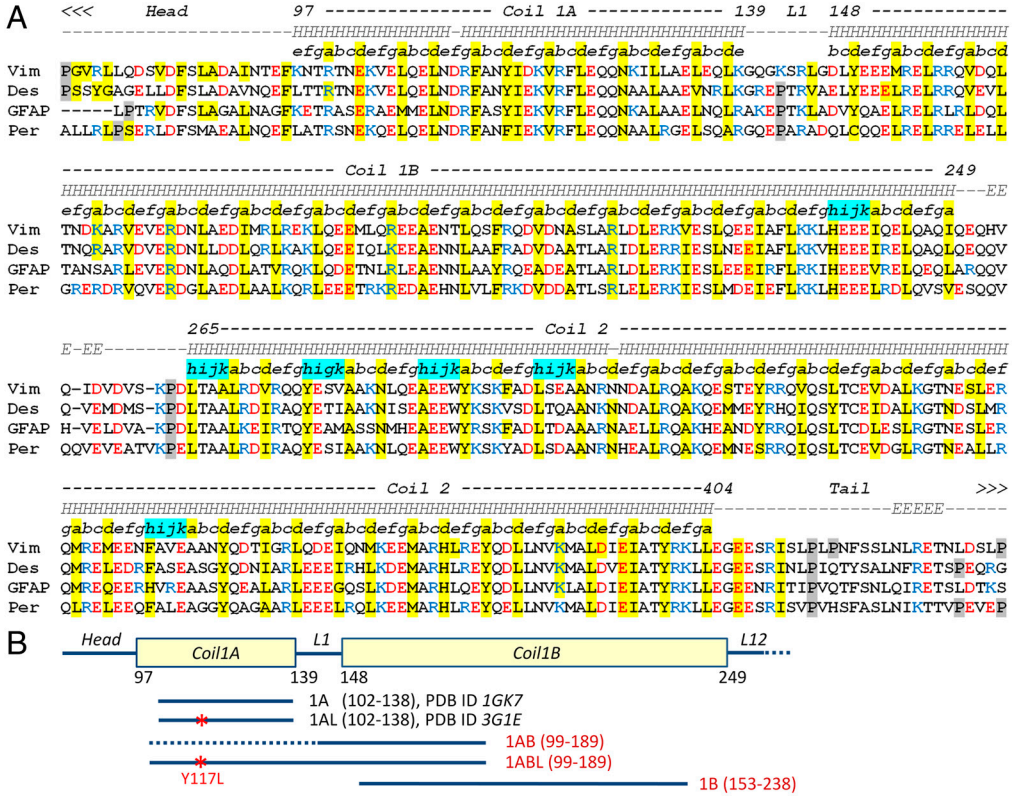

Fig. 1. Primary structure analysis of the IF rod domain. (*A*) Sequence alignment for the rod domains of human type III IF proteins including vimentin, desmin, GFAP, and peripherin. Residues that are predicted by the NetSurfP algorithm (23) to be buried inside the structure are highlighted in yellow. Heptad assignment is indicated. The secondary structure prediction for the vimentin sequence by the Jpred3 algorithm (22) is shown on the *Top* (*H* indicates α-helix, *E* indicates β-sheet). Stutter inserts resulting in 11-residue repeats are highlighted with cyan. Proline residues are highlighted with gray. (*B*) Schematic diagram of coil 1 of human vimentin and its fragments discussed in the text. Yellow rectangles indicate the α-helical regions. The disordered region in the *1AB* fragment structure is indicated by a dashed line. Red star indicates the *Y117L* mutation.

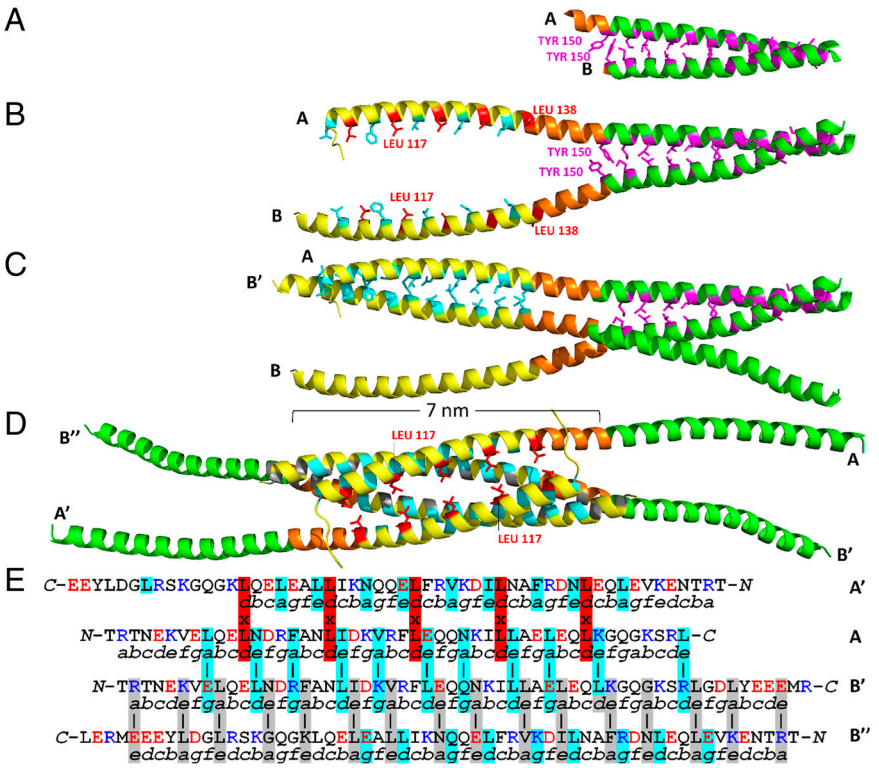

Fig. 2. Crystal structures of the *1AB* and *1ABL* fragments. (*A*) Ribbon diagram of the *1AB* structure. The side chains of residues in heptad positions *a* and *d* are shown in magenta. With the exception of residues 144 to 149 (shown in orange) in chain A, the rest of the linker L1 and coil 1A is disordered in the crystals. Figure drawn using the program Pymol (40). (*B*) Ribbon diagram of the *1ABL* structure showing two chains A and B present in the crystallographic asymmetric unit. The 1A, L1, and 1B parts are colored yellow, orange and green, respectively. Within coil 1A, the residues in predicted heptad positions *a* and *d* (Fig. 1*A*) are shown in cyan and red, respectively (same as in *E* below). Within coil 1B, the residues in both heptad positions *a* and *d* are shown in magenta. The mutated Leu117 residue is labelled. (*C*) Ribbon diagram of the *1ABL* structure showing chains A and B as well as a crystal symmetry-related copy (B′) of the latter. Chains B and B′ make contacts with chain A within coil 1B and coil 1A parts, respectively. The residues that are involved in the interaction of the coil-1A parts of chains A and B′ are shown in cyan; these correspond to heptad positions *a* and *e* in chain A and *g* and *d* in chain B′ (see also *E*). Correspondingly, there is a register shift of one residue between the parallel chains A and B′. (*D*) An antiparallel CC tetramer formed by the 1A parts in the *1ABL* crystals. Chain A′ is a crystal symmetry equivalent of chain A. Chains B′ and B″ are symmetry equivalents of chain B. For clarity, other symmetry-related chains forming the CC within the 1B part are not shown here. The residues involved in the hydrophobic core of the tetramer are shown in red, cyan, and gray according to the pairing indicated in *E*. In particular, the "knobs-to-knobs" interface of the antiparallel chains A and A′ is formed by five Leu residues on each side (all in positions *d*) and is shown with their side chains in red. The interface of antiparallel chains B′ and B′ is of a classical (antiparallel) 'knobs-into-holes' type; it involves the residues in *a* and *e* positions of either chain. (*E*) Alignment of the four 1A parts forming the antiparallel tetramer shown in *D*. The heptad assignment is indicated below each chain. The opposing pairs of residues forming the hydrophobic interactions ("knobs-into-holes") between chains A and B′ and chains A′ and B″ (parallel, one residue register shift) are shown in cyan. Similar interactions formed by chains B and B′ (antiparallel) are highlighted with gray. The knob-to-knob interface of antiparallel chains A and A′ is highlighted with red.

Crystal Structure of the Modified *1AB* Fragment Carrying the *Y117L* Mutation. Since the coil-1A and linker-L1 regions remained unresolved in the crystal structure of the *1AB* fragment, we have prepared a point-mutated variant (termed *1ABL*) which carries the *Y117L* mutation known to radically stabilize the CC formation within coil 1A (27). The obtained *1ABL* crystals diffracted to 2.45 Å resolution and had very different space group and cell parameters than the *1AB* crystals (Table S1). In the asymmetric unit there are two chains (A and B) that are ordered all along their length (Fig. 2*B*). Interestingly, both chains were found to contain an exclusively α-helical structure that continues from the coil-1A part into L1 and coil 1B. The coil-1B parts of chains A and B form the predicted CC, which is essentially identical to the *1AB* fragment structure, as clear from their superimposition (Fig. 3*A*). In both structures the α-helices splay apart upstream of Tyr 150 (hepad position *d*). Because of the rigid α-helical structure of linker L1 in the *1ABL* fragment, this results in a 25 Å separation between the C_α-atoms of Leu138, which is the last predicted core residue of coil 1A in chains A and B (Fig. 3*A*).

However, the arrangement of the 1A parts within the *1ABL* structure is radically different from a parallel CC dimer, even though such a dimer should be very stable and indeed is found in the crystals of the 1A (*Y117L*) fragment (27). Instead, a tetrameric left-handed CC assembly involving 1A helices from crystal symmetry-related molecules is found. The tetramer includes chains A and B′ (being a symmetry equivalent of B) running in one direction (Fig. 2*C*), and chains A′ and B″ (being further symmetry equivalents of A and B respectively) running in the opposite direction (Fig. 2*D*). The tetramer is stabilized by a common hydrophobic core involving residues from all four chains. This stabilization is due to three different types of hydrophobic contacts: between two parallel chains (A and B′), between antiparallel chains A and A′, and between antiparallel chains B′ and B″ (Fig. 2*D*). Unexpectedly, these contacts involve residues in *a* and *d* positions of the predicted heptads but also additional residues in positions *e* and *g* (Fig. 2*E*). Interestingly, altogether the interactions of the 1A and 1B parts lead to the formation of a dodecamer arrangement consisting of six 1B dimers and three 1A tetramers (Fig. S1).

Structure of Coil 1B. For vimentin coil 1B, the α-helical structure is predicted between residues 148 and 249 (Fig. 1*A*). The expected heptad pattern is also reliably confirmed by the NetSufP algorithm with the exception of a single discontinuity, corresponding to a stutter, that appears to be present close to the C terminus of coil 1B at position 238 (Fig. 1*A*). This is a unique feature that was

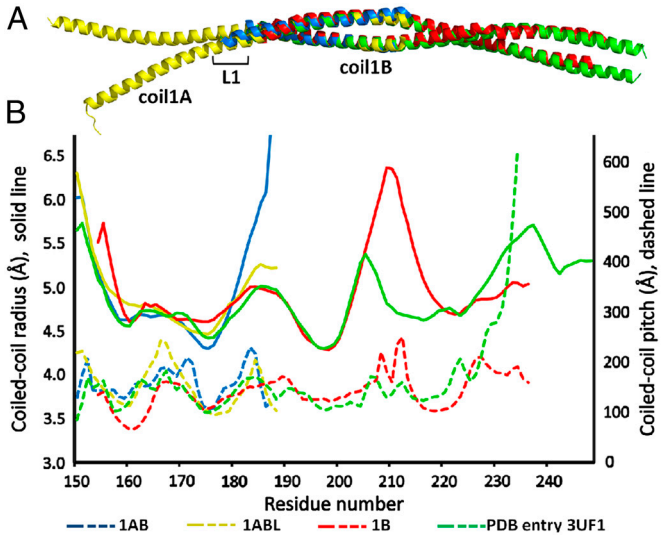

Fig. 3. Complete structure of vimentin coil 1 based on crystal structures. (*A*) Least-squares structural superposition of the *1AB*, *1ABL*, and *1B* fragments as well as the PDB entry *3UF1*. The four structures are shown in blue, yellow, red and green respectively. (*B*) Plots of the CC radius (solid lines) and pitch (dash) as a function of residue number calculated using the program Twister (41). The data for the *1ABL*, *1AB*, *1B*, and *3UF1* structures are shown in the same colors as in *A*.

not detected by the heptad-filtering algorithms before. In the past, we reported diffracting crystals for vimentin fragment including residues 160 to 235 (17), but attempts to phase the structure failed. Now we have prepared a series of vimentin coil-1B fragments with varying N and C termini, yielding diffracting crystals for three fragments 161–238, 161–243, and 153–238, respectively. All three structures could be phased using SeMet SAS. However, the crystal structures of the two former fragments revealed CC trimers rather than the dimers expected for the full-length protein. Only the last fragment including residues 153–238 (denoted *1B*, Fig. 1*B*) formed the expected dimers. Apparently, the first eleven residues of coil 1B are important for the formation of the CC with the correct number of α-helices. The crystal structure of the *1B* fragment at 1.7 Å resolution reveals a regular left-handed CC structure all along its length (Fig. 3*A*), in full agreement with the predicted heptad pattern (Fig. 1*A*).

Discussion

Structural Organization of Vimentin Rod. The obtained X-ray structures reveal the molecular organization of the complete vimentin coil 1. Most interestingly, the crystals of vimentin fragment *1ABL* (carrying the *Y117L* mutation) show a contiguous α-helical structure for coil 1A, linker L1, and the beginning of coil 1B. While the 1B part forms the predicted dimer, the two α-helices splay apart in the linker-L1 region, and the 1A parts become separated (Fig. 2*B*). The *1AB*, *1ABL*, and *1B* structures cover a major part of coil 1B, which should span residues 148 to 249 according to our best prediction. In addition, a further crystal structure of a fragment including vimentin residues 144 to 251—i.e., encompassing the whole coil 1B—and carrying an additional His-tag at the N terminus became recently available (PDB entry *3UF1*). Taken together, the four crystal structures provide a redundant view of the coil 1B. The superposition of all these structures produces a reasonable match (Fig. 3*A*), despite the fact that CCs are generally prone to bending and further distortions due to crystal lattice contacts. A further comparison is provided by the CC geometry analysis (Fig. 3*B*). Here it should be noted that the *3UF1* structure confirms our prediction of a parallel α-helical bundle structure at the very C terminus of coil 1B, resulting from a stutter at position 238 (Fig. 1*A*). Indeed, the CC pitch increases to about 300 Å near residue 231, which is twice the mean value seen for the rest of coil 1B (145 Å), and rapidly becomes infinite, indicating parallel helices. Finally, the *3UF1* structure reveals an α-helical structure starting with residue 144 already—i.e., for a few residues of linker L1—which supports our observation of an α-helical linker L1 in the *1ABL* fragment structure.

Together with our recent results on the complete coil-2 structure (19, 20), the data presented here allow us to reconstruct the vimentin rod in its entire length (Fig. 4*A*). The only region where crystallographic data are currently still missing is the linker L12 (residues 250 to 262). This structure was recently theoretically modelled by Parry and Smith (30). Here, the secondary structure prediction using Jpred3 points to a short stretch of β-conformation (five residues, His253 to Asp257) followed by a presumably flexible region. As a possibility remaining to be proven experimentally, the two short strands from either chain might form an antiparallel β-hairpin in the plane perpendicular to the dimer axis. In summary, the rod domains starts with coil 1A and linker L1, which may represent special, dynamic structures (discussed below), followed by two stable CC segments—i.e., coil 1B and coil 2—joined by the linker L12. Most of this CC structure has a classical left-handed geometry (Fig. 4*A*), but the CC unwinds at several places due to the presence of stutter inserts in the amino acid sequence (Fig. 1*A*). One such insert is present near the end of coil 1B, four inserts locate near the beginning of coil 2 (resulting in a parallel α-helical "bundle"), and one roughly in the middle of coil 2.

IF Tetramer Structure. Based on the 3D structure of the complete dimeric rod, a reliable model of a tetramer, the soluble vimentin species, becomes within reach (Fig. 4*B*). While originally established using cross-linking studies (10), the relative position of the two oppositely oriented dimers within an A_{11}-type tetramer was recently further refined by spin-labelling and electron paramagnetic resonance (EPMR) studies (11), showing that the residues Glu191 are aligned. Interestingly, the crystal structure of the vimentin fragment corresponding to the complete coil 1B (PDB entry *3UF1*) contains two antiparallel dimers per asymmetric unit that show this exact alignment. We have used this crystal structure as a template to build the full tetramer—save the non-α-helical head and tail domains (Fig. 4*B*). Within our tetramer model, the α-helical linkers L1 of one dimer are roughly aligned with the C-terminal part of coil 1B of the antiparallel dimer. As the rod domain is generally quite polar except for the core residues (Fig. 1*A*), analysis of the adjacent surfaces of the two dimers in the modelled tetramer does not reveal significant hydrophobic patches or shape complementarity. However, there is a distinct complementarity in the charge distribution on adjacent surfaces (Fig. 4*C*). The involvement of charge complimentarity in tetramer formation was suggested earlier based on the aminoacid sequence (31, 32). As the most striking feature, the last coil-1A residue Lys139 and the linker L1 (140-GQGKSRLG-147, positively charged) of one dimer are found aligned with the C terminus of coil 1B of the antiparallel dimer (238-HEEEIQELQAQI-249, negatively charged) (Fig. 4 *C* and *D*).

It should be noted that the head domain plays an essential role in the tetramer formation, as both the "headless" vimentin and isolated vimentin rod stay dimeric in the standard low-molarity buffer (5 mM Tris-HCl, pH 8.4) (7). The head's involvement appears to be based on the attraction between the eleven arginines, which are the only charged residues within the first 80 residues of vimentin sequence, and the acidic rod (5). We hypothesize that the complementary charge patterns of the rod domains discussed here, while being insufficient alone to drive the stable tetramer formation, may be important for defining the correct register of the A_{11} tetramer.

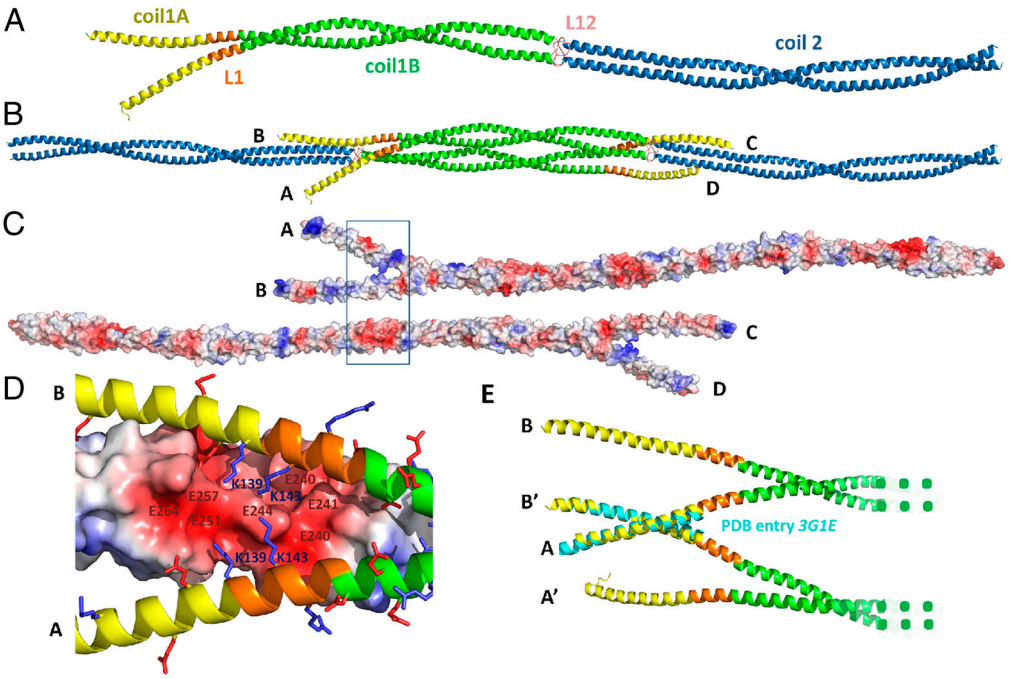

Fig. 4. Vimentin tetramer structure and lateral association mechanism. (*A*) Three-dimensional structure of vimentin dimer. The coil-1 structure (with coil 1A, L1, and coil 1B shown in yellow, orange, and green, respectively) is based on the superposition of the crystal structures shown in Fig. 3*A*. Similarly, the coil-2 structure (blue) is a superposition of previously established fragment structures (19, 42). The linker L12 for which no crystallographic data are available yet is shown schematically in pink. In the full dimer, the rod domain is flanked by the flexible head and tail domains, also without crystallographic information. (*B*) Three-dimensional structure of vimentin tetramer. Two antiparallel dimers were aligned in the A_{11} mode following the tetrameric arrangement seen in the crystal structure (PDB entry *3UF1*). (*C*) Molecular surfaces of two vimentin dimers forming the tetramer, colored by electrostatic potential (as estimated using the program Pymol). Blue and red coloring corresponds to positive and negative potential, respectively. Compared to *B*, one dimer (CD) was rotated by approximately 20° about the horizontal axis to reveal the surface facing the other dimer. The surface representation of this other dimer (AB) was additionally rotated by 180° to reveal the surface facing the dimer CD. The rectangle indicates the interaction areas presented in *D*. (*D*) Zoom-in to the interactions between the linker L1 region of chains A and B (shown as ribbons) and the C-terminus of coil 1B of dimer CD (shown as surface colored by electrostatic potential). All charged side groups of chains A and B are shown as sticks. (*E*) A possible involvement of parallel coil-1A segments in higher lateral assembly (octamers and beyond). If two tetramers ABCD and A′B′C′D′ (*B*) are laterally aligned, the dimers that run parallel to each other (AB and A′B′) may interact via a "cross-coil" formation of the coil-1A segments. This possibility is demonstrated by fitting the coil-1A parts of chains A and B′ on either chain of the dimeric coil-1A (*Y117L*) structure (PDB entry *3G1E*, cyan).

Role of Coil 1A and Linker L1 in IF Assembly. The coil-1A fragment of vimentin was present as a monomer in crystals (18), and it exhibited only a weak CC-forming capacity, as manifested by its low thermal stability (melting temperature $T_m = 32\,°C$ at 1 mg/ml concentration) (27). However, the CC formation within this fragment can be drastically stabilized by a point mutation *Y117L* (leading to $T_m = 71\,°C$) (27), which replaces the bulky Tyr side chain in a core CC position (*d*) by a favorable Leu residue. Moreover, the full-length vimentin *Y117L* mutant does not assemble beyond the ULF stage both in vitro and in cDNA-transfected cultured cells (27, 33). These observations led to suggest that coil 1A may serve as a dynamic "switch" with the functionally significant property to alternate between a monomeric helix and a CC dimer depending on the particular IF assembly stage (27, 34). Interestingly, our modelling work presented here (Fig. 4*B*) indicates that within the A_{11} tetramer the coil-1A parts of one dimer are roughly aligned with the parallel bundle at the N terminus of coil 2 of the other dimer. Whether or not there is a direct interaction between these antiparallel α-helical elements is a question still to be answered. As a further remark, once A_{11}-type tetramers stack laterally, a CC formation by the 1A helices coming from two different dimers becomes feasible (Fig. 4*E*). We hypothesize that this situation, which we here denote as the "cross-coil," indeed could take place at the ULF stage and/or in mature filaments. The cross-coil formation, just like an intradimeric CC, would correspond to the proximity of spin-labelled residues in *a* and *d* positions within coil 1A of full-length vimentin, as suggested from the broadening of the corresponding EPMR spectra (35). This possibility may explain the lack of longitudinal assembly of the *Y117L* mutant (27, 33), since the formation of cross-coils should act as a topological hurdle.

Our crystallographic data on the *1ABL* fragment reveal that the vimentin linker L1 can accommodate a fully α-helical conformation. This unexpected observation deviates from secondary structure predictions that indicated the interruption of the α-helical structure at L1. In addition, unlike human vimentin, desmin, GFAP, and peripherin all contain a proline residue (Pro) within L1 (Fig. 1*A*); a Pro in the same position is also found in vimentin of electric ray *Torpedo californica* (36). When embedded in an α-helical structure, Pro residues result in a destabilizing kink (37). Helix formation within the linker-L1 region should be therefore best considered a possibility rather than a rule. Importantly, there must be an interplay between the coil-1A and linker-L1 dynamics. Indeed, if linker L1 stays fully α-helical, this will not allow the 1A parts to zip into a CC within the same full-length vimentin dimer (see Fig. 2*B*). At the dimer stage, the tendency of the α-helix to extend into the linker L1 may overweigh the weak propensity of coil 1A to zip into an (intradimeric) CC, which are mutually exclusive possibilities.

In conclusion, there appears to be a number of rather delicate "switches" that control the normal IF assembly at the molecular level. Firstly, the assembly does not proceed unless the basic head domain interacts with the acidic rod. Secondly, the assembly may involve the dynamic alternation of coil-1A conformation between a CC and a monomeric helix. As a parallel effect, the linker L1 could accommodate α-helical conformation at some stages of IF

assembly, possibly including the final compacted filament, but yet any excessive stabilization of this conformation has a detrimental effect on the assembly process. Finally, the linker L1 and coil 1B reveal a charge distribution pattern that promotes the proper A_{11}-mode alignment of two antiparallel dimers, in line with earlier predictions (31, 32).

Materials and Methods

Molecular Cloning. Vimentin fragment *1AB* was cloned into the vector pPEP-TEV that allows the overexpression of a fusion construct including an N-terminal His_6-tag, a 5-kDa laminin spacer, a TEV protease cleavage site, and the sequence of interest (38). Thereafter the point mutation *Y117L* was introduced to create the construct expressing the *1ABL* fragment. All coil-1B fragments were inserted into the pETHSUL vector (39), resulting in fusion products containing a His_6-tag, the SUMO sequence, the SUMO protease cleavage site and the vimentin fragment.

Protein Expression and Purification. After expression of the fusion constructs in *E.coli* BL21(DE3) culture, the soluble protein fraction was collected. The following purification procedure included the first affinity chromatography step on a Ni-chelating column that retained the fusion, the cleavage at the TEV/SUMO protease site, a second Ni-chelating column that separated the vimentin fragment from the free tag and the uncleaved fusion, and the final gel-filtration step. Selenomethionine-labelled fragments were obtained using SeMet-containing growth medium, and purified using the same procedure as the native fragments. Obtained fragments *1AB* and *1ABL* carried two exogenous amino acids (GS) at the N terminus due to the TEV protease cleavage site. The fragment *1B* started directly from the vimentin sequence.

Crystal Structure Determination. Crystallization conditions were found using sparse matrix sampling, and further improved using systematic optimization. The final crystallization conditions are given in Table S1. Diffraction data were collected using synchrotron radiation source. Experimental phases for all fragments were determined based on the anomalous scattering from the SeMet-containing crystals, followed by the atomic model building. The final models for the *1AB* and *1ABL* fragments were refined using the data collected from the native crystals. The crystals of the native *1B* fragment did not diffract well, and the SeMet crystal data were used for refinement. The quality parameters of the final models are provided in Table S1.

For detailed Materials and Methods, see the *SI Text*.

ACKNOWLEDGMENTS. Authors thank Dr. Stephen Weeks for providing the pETHSUL expression vector and for stimulating discussions, and Mr. Steven Beelen for technical assistance. We are also grateful to Prof. J. Rozensky for mass-spectrometry analysis, to Drs. Beatriz Guimaraes, Andrew W. Thompson, and Kristof Van Hecke for help with X-ray data collection, and to Dr. John F. Hunt and colleagues from the Northeast Structural Genomics Consortium for making their structure 3UF1 available in the PDB prior to publication. Measurements at the Soleil synchrotron (beamline Proxima1) and at the Swiss Light Source (beamline PXIII) were supported by the European Commission under the 7th Framework Programme. This work was supported by the Katholieke Universiteit Leuven Onderzoekstoelage Grant 07/071, by the Research Foundation - Flanders (FWO) Grant G.0709.12 (both to S.V.S.) and by the German Research Foundation, DFG BA 2186/3-1 (to H.H.).

1. Fuchs E, Weber K (1994) Intermediate filaments: Structure, dynamics, function, and disease. *Annu Rev Biochem* 63:345–382.
2. Herrmann H, Bar H, Kreplak L, Strelkov SV, Aebi U (2007) Intermediate filaments: From cell architecture to nanomechanics. *Nat Rev Mol Cell Biol* 8:562–573.
3. Lazarides E (1982) Intermediate filaments: A chemically heterogeneous, developmentally regulated class of proteins. *Annu Rev Biochem* 51:219–250.
4. Herrmann H, Hesse M, Reichenzeller M, Aebi U, Magin TM (2003) Functional complexity of intermediate filament cytoskeletons: From structure to assembly to gene ablation. *Int Rev Cytol* 223:83–175.
5. Herrmann H, Aebi U (2004) Intermediate filaments: Molecular structure, assembly mechanism, and integration into functionally distinct intracellular scaffolds. *Annu Rev Biochem* 73:749–789.
6. Parry DA (1982) Coiled-coils in alpha-helix-containing proteins: Analysis of the residue types within the heptad repeat and the use of these data in the prediction of coiled-coils in other proteins. *Biosci Rep* 2:1017–1024.
7. Herrmann H, et al. (1996) Structure and assembly properties of the intermediate filament protein vimentin: The role of its head, rod, and tail domains. *J Mol Biol* 264:933–953.
8. Lichtenstern T, Mucke N, Aebi U, Mauermann M, Herrmann H (2012) Complex formation and kinetics of filament assembly exhibited by the simple epithelial keratins K8 and K18. *J Struct Biol* 177:54–62.
9. Steinert PM, Marekov LN, Fraser RD, Parry DA (1993) Keratin intermediate filament structure: Crosslinking studies yield quantitative information on molecular dimensions and mechanism of assembly. *J Mol Biol* 230:436–452.
10. Steinert PM, Marekov LN, Parry DA (1993) Diversity of intermediate filament structure: Evidence that the alignment of coiled-coil molecules in vimentin is different from that in keratin intermediate filaments. *J Biol Chem* 268:24916–24925.
11. Hess JF, Budamagunta MS, Voss JC, FitzGerald PG (2004) Structural characterization of human vimentin rod 1 and the sequencing of assembly steps in intermediate filament formation in vitro using SDSL and EPR. *J Biol Chem* 279:44841–44846.
12. Mucke N, et al. (2004) Molecular and biophysical characterization of assembly-starter units of human vimentin. *J Mol Biol* 340:97–114.
13. Quax-Jeuken YE, Quax WJ, Bloemendal H (1983) Primary and secondary structure of hamster vimentin predicted from the nucleotide sequence. *Proc Natl Acad Sci USA* 80:3548–3552.
14. Strelkov SV, Herrmann H, Aebi U (2003) Molecular architecture of intermediate filaments. *Bioessays* 25:243–251.
15. Parry DAD, Steinert PM (1999) Intermediate filaments: Molecular architecture, assembly, dynamics, and polymorphism. *Q Rev Biophys* 32:99–187.
16. Omary MB (2009) "IF-pathies": A broad spectrum of intermediate filament-associated diseases. *J Clin Invest* 119:1756–1762.
17. Strelkov SV, et al. (2001) Divide-and-conquer crystallographic approach towards an atomic structure of intermediate filaments. *J Mol Biol* 306:773–781.
18. Strelkov SV, et al. (2002) Conserved segments 1A and 2B of the intermediate filament dimer: Their atomic structures and role in filament assembly. *EMBO J* 21:1255–1266.
19. Nicolet S, Herrmann H, Aebi U, Strelkov SV (2010) Atomic structure of vimentin coil 2. *J Struct Biol* 170:369–376.
20. Chernyatina AA, Strelkov SV (2012) Stabilization of vimentin coil-2 fragment via an engineered disulfide. *J Struct Biol* 177:46–53.
21. Dhe-Paganon S, Werner ED, Chi YI, Shoelson SE (2002) Structure of the globular tail of nuclear lamin. *J Biol Chem* 277:17381–17384.
22. Cole C, Barber JD, Barton GJ (2008) The Jpred 3 secondary structure prediction server. *Nucleic Acids Res* 36:W197–W201.
23. Petersen B, Petersen TN, Andersen P, Nielsen M, Lundegaard C (2009) A generic method for assignment of reliability scores applied to solvent accessibility predictions. *BMC Struct Biol* 9:51.
24. Lupas A (1997) Predicting coiled-coil regions in proteins. *Curr Opin Struct Biol* 7:388–393.
25. Gruber M, Lupas AN (2003) Historical review: Another 50th anniversary—new periodicities in coiled coils. *Trends Biochem Sci* 28:679–685.
26. Kuhnel K, et al. (2004) The VASP tetramerization domain is a right-handed coiled coil based on a 15-residue repeat. *Proc Natl Acad Sci USA* 101:17027–17032.
27. Meier M, et al. (2009) Vimentin coil 1A-A molecular switch involved in the initiation of filament elongation. *J Mol Biol* 390:245–261.
28. Brown JH, Cohen C, Parry DA (1996) Heptad breaks in alpha-helical coiled coils: Stutters and stammers. *Proteins* 26:134–145.
29. Smith TA, Strelkov SV, Burkhard P, Aebi U, Parry DA (2002) Sequence comparisons of intermediate filament chains: Evidence of a unique functional/structural role for coiled-coil segment 1A and linker L1. *J Struct Biol* 137:128–145.
30. Parry DA, Smith TA (2010) A different conformation for linker L12 in IF molecules in the molecular and filamentous forms: An hypothesis. *J Struct Biol* 170:364–368.
31. Parry DA, Crewther WG, Fraser RD, MacRae TP (1977) Structure of alpha-keratin: Structural implication of the amino acid sequences of the type I and type II chain segments. *J Mol Biol* 113:449–454.
32. McLachlan AD, Stewart M (1982) Periodic charge distribution in the intermediate filament proteins desmin and vimentin. *J Mol Biol* 162:693–698.
33. Georgakopoulou S, Moller D, Sachs N, Herrmann H, Aebi U (2009) Near-UV circular dichroism reveals structural transitions of vimentin subunits during intermediate filament assembly. *J Mol Biol* 386:544–553.
34. Smith TA, Strelkov SV, Burkhard P, Aebi U, Parry DA (2002) Sequence comparisons of intermediate filament chains: Evidence of a unique functional/structural role for coiled-coil segment 1A and linker L1. *J Struct Biol* 137:128–145.
35. Aziz A, Hess JF, Budamagunta MS, FitzGerald PG, Voss JC (2009) Head and rod 1 interactions in vimentin: Identification of contact sites, structure, and changes with phosphorylation using site-directed spin labeling and electron paramagnetic resonance. *J Biol Chem* 284:7330–7338.
36. Schaffeld M, Herrmann H, Schultess J, Markl J (2001) Vimentin and desmin of a cartilaginous fish, the shark Scyliorhinus stellaris: Sequence, expression patterns, and in vitro assembly. *Eur J Cell Biol* 80:692–702.
37. Barlow DJ, Thornton JM (1988) Helix geometry in proteins. *J Mol Biol* 201:601–619.
38. Strelkov SV, Kreplak L, Herrmann H, Aebi U (2004) Intermediate filament protein structure determination. *Methods Cell Biol* 78:25–43.
39. Weeks SD, Drinker M, Loll PJ (2007) Ligation independent cloning vectors for expression of SUMO fusions. *Protein Expr Purif* 53:40–50.
40. DeLano WL (2002) *The PyMOL User's Manual* (DeLano Scientific, San Carlos, CA).
41. Strelkov SV, Burkhard P (2002) Analysis of alpha-helical coiled coils with the program TWISTER reveals a structural mechanism for stutter compensation. *J Struct Biol* 137:54–64.
42. Chernyatina AA, Strelkov SV (2012) Stabilization of vimentin coil-2 fragment via an engineered disulfide. *J Struct Biol* 177:46–53.